Faraday Discussions

Cite this: DOI: 10.1039/d0fd00049c

PAPER

View Article Online
View Journal

Published on 02 June 2020. Downloaded by RUTGERS STATE UNIVERSITY on 9/24/2020 8:27:22 PM.

Developing new and understanding old approximations in TDDFT

Lionel Lacombe and Neepa T. Maitra

Received 29th April 2020, Accepted 2nd June 2020

DOI: 10.1039/d0fd00049c

When a system has evolved far from a ground-state, the adiabatic approximations commonly used in time-dependent density functional theory calculations completely fail in some applications, while giving qualitatively good predictions in others, and sometimes even quantitative predictions. It is not clearly understood why this is so, and developing practical approximations going beyond the adiabatic approximation remains a challenge. This paper explores three different lines of investigation. First, an expression for the exact time-dependent exchange–correlation potential suggests that the accuracy of an adiabatic approximation is intimately related to the deviation between the natural orbital occupation numbers of the physical system and those of the Kohn–Sham system, and we explore this on some exactly-solvable model systems. The exact expression further suggests a path to go beyond the adiabatic approximations, and in the second part we discuss a newly proposed class of memory-dependent approximations developed in this way. Finally, we derive a new expression for the exact exchange–correlation potential from a coupling-constant path integration.

Time-dependent density functional theory (TDDFT) continues to be a method of choice for the calculation of electronic spectra and dynamics of molecules and solids, where its favorable system-size scaling enables computations on large systems that could not be done otherwise.[1–4] An area of application that particularly demonstrates this is non-adiabatic electron–ion dynamics, which requires efficient and accurate electronic structure methods to be used on the fly with nuclear trajectories evolving in a high-dimensional space. An illustrative recent example is the photo-induced dynamics of the rotary molecular machines and 1- and 3-pore covalent organic frameworks in ref. 5 which involved up to 600 atoms, a feat which would be a challenge for any alternative electronic structure method of similar accuracy, even with the GPU acceleration that was used. The real-time TDDFT equations are highly scalable and parallelizable, as demonstrated, in another example, by the first-principles calculations of electronic stopping power and conductivity in a system of 5400 disordered Al atoms (59 400 electrons).[6]

Department of Physics, Rutgers University, Newark, New Jersey 07102, USA. E-mail: neepa.maitra@rutgers.edu; liolacombe@gmail.com

Published on 02 June 2020. Downloaded by RUTGERS STATE UNIVERSITY on 9/24/2020 8:27:22 PM.

There are in fact very few practical alternatives to TDDFT for dynamics when the electronic system is driven far from any ground-state, such as when driven by a strong external field, or when prepared in a superposition state. In this regime, recent work on model systems shows that the exact exchange–correlation (XC) potential typically exhibits large dynamical features that the approximations commonly used in calculations cannot capture, *e.g.* ref. 7–14. These approximations are “adiabatic”, meaning that they input the instantaneous density into a chosen ground-state approximation, while it is known that the exact XC potential depends on the history of the density, as well as the initial interacting and Kohn–Sham states. Due to its lack of this memory, the adiabatic approximation completely fails in some applications, *e.g.* ref. 15–21. Yet, in other cases, the adiabatic approximation is found to give good predictions. The adiabatic approximation is derived under the condition of an initial ground-state subject to a slowly-varying perturbation, which is hardly the situation in most of the applications considered. For example, quite often TDDFT simulates dynamics after a photo-excitation in a molecule (*e.g.* in photovoltaic applications) where the initial state is excited, *e.g.* ref. 5, 22 and 23. In other applications, the system starts in a ground-state but is driven by a strong laser field, *e.g.* ref. 24–26. These are hardly in an adiabatic regime. Why and when does adiabatic TDDFT give even qualitatively correct predictions, let alone quantitatively useful results? It is true that its complete neglect of memory results in the satisfaction of a number of exact conditions that are important in the time-dependent case,[27,28] but a characterization of when it is expected to work well is lacking. How can we derive approximations that include memory while also satisfying exact conditions that are important for the time-dependent case?

In this paper we take walks along three paths to investigate these questions, guided by exact expressions for the XC potential. First, decomposing the XC potential into a part depending on the kinetic term and one depending on the interaction term hints to us that when the natural orbital occupation numbers of the physical system begin relatively close to those of the Kohn–Sham system and do not change significantly during the dynamics, the adiabatic approximations could give reasonable results provided the dynamics does not critically rely on the resonant frequencies of the system. Such a situation can encompass dynamics far from any ground-state, and we show (Sec. 2), using model systems, that then even ALDA can predict the dynamics well. This is especially true when only spatially-averaged observables such as the dipole moment are of interest. The choice of initial KS state is critical: if this is chosen to have a configuration similar to that of the physical system, non-adiabatic features such as steps and peaks can be minimized. However, when the true dynamics is such that its natural orbital occupation numbers change significantly with time, or when the dynamics depends critically on the resonant frequencies, approximations going beyond the adiabatic ones are required, and this leads us to the second path: developing approximations based on the exact decomposition (Sec. 3). Facing some numerical up-hills along this path, we take a different path in Sec. 4, exploring the use of a coupling-constant integration to transform away the challenging kinetic term.

Published on 02 June 2020. Downloaded by RUTGERS STATE UNIVERSITY on 9/24/2020 8:27:22 PM.

1 The exact XC potential

TDDFT calculations proceed by solving for non-interacting electrons, beginning in an initial state $\Phi(\mathbf{r}_1,\ldots\mathbf{r}_N,0)$, and evolving in a one-body potential, $v_{\text{ext}}(\mathbf{r},t) + v_{\text{H}}(\mathbf{r},t) + v_{\text{XC}}(\mathbf{r},t)$ where v_{ext} is the potential from the nuclei plus any externally applied fields, $v_{\text{H}}(\mathbf{r},t) = \int dr' w(|\mathbf{r}-\mathbf{r}'|)n(\mathbf{r}',t)$ is the Hartree potential for the two-body electron interaction w, and $v_{\text{XC}}(\mathbf{r},t) = v_{\text{XC}}[n;\,\Psi_0,\Phi_0](\mathbf{r},t)$ is the XC potential, a functional of the density, including its history, the physical initial state of the system $\Psi(0)$ and the KS initial state $\Phi(0)$. The state $\Phi(0)$ can be chosen quite freely, but subject to the condition that its initial one-body density $n(\mathbf{r},0)$ and the first time-derivative $\dot{n}(\mathbf{r},0)$ coincide with those of the initial interacting state. The XC potential $v_{\text{XC}}(\mathbf{r},t)$ depends heavily on this choice.

An exact expression for the XC potential arises from equating $\ddot{n}(\mathbf{r},t)$ in the Kohn–Sham (KS) system to that of the true system. This yields a "force-balance" equation[29–31] for the exact XC potential:

$$\nabla\cdot(n\nabla v_{\text{XC}}) = \nabla\cdot(n(\mathbf{r},t)\nabla v_{\text{XC}}^{\text{W}}(\mathbf{r},t)) + \nabla\cdot(n(\mathbf{r},t)\nabla v_{\text{C}}^{\text{T}}(\mathbf{r},t)) \tag{1}$$

where the interaction component v_{XC}^{W} satisfies

$$\nabla\cdot\left(n\nabla v_{\text{XC}}^{\text{W}}\right) = \nabla\cdot\left[n(\mathbf{r},t)\int n_{\text{XC}}(\mathbf{r}',\mathbf{r},t)\nabla w(|\mathbf{r}'-\mathbf{r}|)\mathrm{d}^3r'\right], \tag{2}$$

and the kinetic component v_{C}^{T} satisfies:

$$\nabla\cdot\left(n\nabla v_{\text{C}}^{\text{T}}\right) = \nabla\cdot\left[\mathscr{D}\left(\rho_1(\mathbf{r}',\mathbf{r},t) - \rho_{1,\text{S}}(\mathbf{r}',\mathbf{r},t)\right)\big|_{\mathbf{r}'=\mathbf{r}}\right], \tag{3}$$

with $\mathscr{D} = \frac{1}{4}(\nabla' - \nabla)(\nabla^2 - \nabla'^2)$. Above, n_{XC} is the time-dependent XC hole defined as

$$n_{\text{XC}}(\mathbf{r},\mathbf{r}',t) = \rho_2(\mathbf{r},\mathbf{r}';\mathbf{r},\mathbf{r}',t)/n(\mathbf{r}',t) - n(\mathbf{r},t), \tag{4}$$

where the two-body reduced density-matrix (2RDM) $\rho_2(\mathbf{r}_1,\mathbf{r}_2,\mathbf{r}_1',\mathbf{r}_2',t) = N(N-1)\int dr_3\ldots dr_N \Psi^*(\mathbf{r}_1',\mathbf{r}_2',\mathbf{r}_3,\ldots\mathbf{r}_N,t)\Psi(\mathbf{r}_1,\mathbf{r}_2,\mathbf{r}_3,\ldots\mathbf{r}_N,t)$, the one-body reduced density matrix (1RDM) $\rho_1(\mathbf{r},\mathbf{r}',t) = N\int dr_2\ldots dr_N \Psi^*(\mathbf{r}',\mathbf{r}_2,\ldots\mathbf{r}_N,t)\Psi(\mathbf{r},\mathbf{r}_2,\ldots\mathbf{r}_N,t)$, and $\rho_{1,\text{S}}$ is the 1RDM of the KS system.

From the form of eqn (2) and (3) above, one expects that v_{XC}^{W} has a relatively smooth form where the integral could be relatively forgiving to approximations of the integrand. On the other hand, the multiple gradients in the expression for v_{C}^{T} may create relatively rapidly varying structures, enhanced at minima of the density, and v_{C}^{T} appears to be far more sensitive to approximations of the 1RDM than v_{XC}^{W} would be to the XC hole. These expectations are borne out in numerical examples on model systems for which the exact XC potential and its decomposition can be calculated, as in ref. 27, 30 and 32. Typically, while v_{XC}^{W} mostly cradles the density in a well that tends to fall off to zero as $-1/r$ asymptotically, v_{C}^{T} displays peak and step structures that often dominate the form of v_{XC}.

In Fig. 1 we give one example to illustrate this; it is a snapshot taken during a key part of the process of scattering of one electron from a hydrogen atom, a problem studied in ref. 10, 33 and 34 using a one-dimensional (1D) model. Specifically, the electrons interact *via* a softened Coulomb potential, $w = 1/\sqrt{(x_1-x_2)^2+1}$, and $v_{\text{ext}}(x) = -1/\sqrt{(x+10)^2+1}$ is used to represent a hydrogen atom at $x = -10$ a.u.,

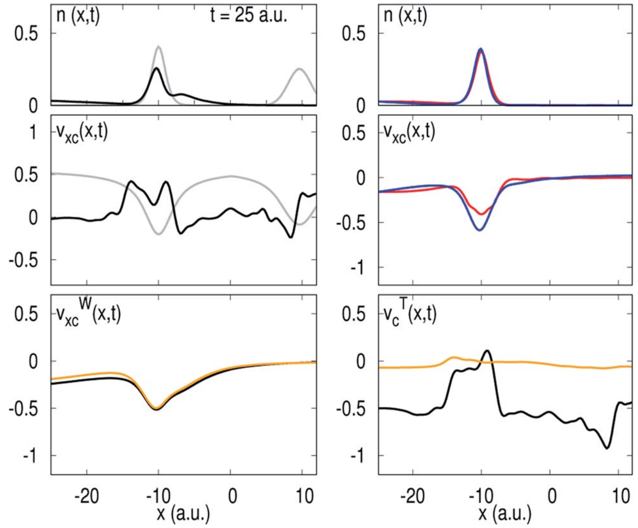

Fig. 1 1D e-H scattering problem. A snapshot in time is shown of the exact density (black) in the top left panel, at a time where the electron is beginning to reflect from the H atom target and partially transmit on the right. In grey is the initial density, for reference. The middle left panel shows the exact XC potential at this time, and that at the initial time is shown in grey. Notably, the peak and step down to the right at $x = -10$ a.u. is a crucial and persistent structure that is responsible for the scattering, and is completely missing in the adiabatic approximations. The top and middle right panels show the density and XC potential obtained from LDA (red) and $v_{\rm XC}^{\rm S}$ (blue) approximations, neither of which yield significant electron reflection. In the lower left panel, the exact $v_{\rm XC}^{\rm W}$ component (black) is well approximated by the best adiabatic approximation of this term, AE (orange), while on the right, the AE approximation of $v_{\rm C}^{\rm T}$ does a poor job of capturing the structure of the exact $v_{\rm C}^{\rm T}$; in particular it is missing the essential feature that induces the reflection.

initially with one electron in its ground-state, $\phi_{\rm H}(x)$, and the other electron as a Gaussian wavepacket incoming from the right, $\phi_{\rm in}(x) = (0.2/\pi)^{1/4} e^{-0.2(x-10)^2 - i1.5(x-10)}$. While in the exact dynamics, there is about a 20% probability of electron reflection, ref. 10 and 33 found that adiabatic approximations were simply unable to capture any noticeable reflection, as the ground-state approximations underlying these do not capture the peak and step/valley structures, shown in a snapshot in Fig. 1, which are essential for splitting off part of the electron density. It is clear that the structure in $v_{\rm C}^{\rm T}$ is crucial for the scattering process. The small peak and step down just to the right of $x = -10$ a.u. persists in time and contains the effective correlation needed for reflecting part of the density of the two non-interacting electrons. The adiabatically-exact (AE) approximation, defined by $v_{\rm XC}^{\rm AE} = v_{\rm XC}^{\rm g.s.}[n(t)](\mathbf{r})$, where g.s. denotes the exact ground-state functional, is the "best" adiabatic approximation in the sense that the only error in it arises from making the adiabatic approximation, rather than from additional approximations from the choice of ground-state approximation. The $v_{\rm XC}^{\rm AE}$ can be analogously decomposed into kinetic and interaction components, and it is clear from the figure that the AE approximation of $v_{\rm C}^{\rm T}$ is far poorer than that of $v_{\rm XC}^{\rm W}$.

The figure also plots a non-adiabatic approximation introduced in several recent reports,[10,27,35] denoted by $v_{\rm XC}^{\rm S}$, which replaces the exact XC hole with the KS hole in $v_{\rm XC}^{\rm W}$. This yields quite a reasonable and practical approximation of that

Published on 02 June 2020. Downloaded by RUTGERS STATE UNIVERSITY on 9/24/2020 8:27:22 PM.

Published on 02 June 2020. Downloaded by RUTGERS STATE UNIVERSITY on 9/24/2020 8:27:22 PM.

term. In general, v_{XC}^{S} is not an adiabatic approximation, since the orbital-dependence of the KS hole makes it implicitly depend on the history of the density. This is true even for two electrons, except when the initial KS state is a spin-singlet chosen to be a single doubly-occupied orbital, in which case v_{XC}^{S} reduces to the exact exchange, v_X.

The choice of the KS initial state directly affects the structure of both v_{XC}^{W} and v_C^T. In particular, v_C^T can be reduced, at least at short times, by choosing an initial KS state "close" to the true initial state.[10,35,36] In the plots above we have chosen the initial KS state to be identical to the true initial state, which is a natural choice for the scattering of one electron from a one-electron atom, for which the spatial part of the wavefunction is $\Phi(0) = \Psi(0) = (\phi_H(x_1)\phi_{in}(x_2) + \phi_{in}(x_1)\phi_H(x_2))/\sqrt{2}$. The results for another natural choice, a Slater determinant, were shown in ref. 10, and this would be an appropriate choice if the system had begun with two electrons in the atom, and had been subject to a laser field that had caused the ionization of one electron, which is now returning to re-scatter off the parent ion when the field cycle changes sign. With this choice, even from the beginning, large step structures appear in v_{XC} which are missing in the approximations, with grave consequences for the dynamics even at early times, yielding incorrectly oscillating densities. Again it is the kinetic component, v_C^T in which these structures appear.

2 Role of time-dependent natural orbital occupation numbers in the accuracy of ALDA

The observations in Sec. 1 suggest that an adiabatic approximation would have the most chance of predicting reasonably accurate dynamics in cases where the near-diagonal elements of the KS 1RDM remain close to the true 1RDM throughout the dynamics, so that the peak and step structures of the exact potential, appearing in the v_C^T component, do not get large. The XC effects contained in v_{XC}^{W} would still play an important part in the dynamics, but as this term is less sensitive to approximations made for the XC hole, the idea is that such approximations could at least qualitatively work well. To investigate this further, consider now the natural orbital expansion,

$$\rho_1(\mathbf{r},\mathbf{r}',t) = \sum_i \eta_i(t)\psi_i^*(\mathbf{r}',t)\psi_i(\mathbf{r},t), \quad \text{with} \sum_i \eta_i(t) = N, \tag{5}$$

for the physical 1RDM, where both the natural orbitals $\psi_i(\mathbf{r},t)$ and their occupation numbers $\eta_i(t)$ are generally time-dependent. In contrast, in the expansion for the KS 1RDM, $\rho_{1,S}(\mathbf{r},\mathbf{r}',t) = \sum_i \eta_{S,i}\phi_i^*(\mathbf{r}',t)\phi_i(\mathbf{r},t)$, the KS natural orbitals are equal to the KS orbitals, and their occupation numbers $\eta_{S,i}$ are constant in time, fixed at the initial time when the KS initial state is chosen, due to the one-body nature of the KS evolution. In terms of the natural orbital expansion then, we can write

$$\begin{aligned}\nabla\cdot\left(n(\mathbf{r},t)v_C^T(\mathbf{r},t)\right) &= \sum_i \eta_i(t)\frac{\nabla^2}{4}\left(4|\nabla\psi_i|^2 - \nabla^2|\psi_i|^2\right) \\ &\quad - \sum_i \eta_{S,i}\frac{\nabla^2}{4}\left(4|\nabla\phi_i|^2 - \nabla^2|\phi_i|^2\right)\end{aligned} \tag{6}$$

What is common in the two 1RDMs is their diagonal value, equal to the one-body density; the differences in their deviations away from the diagonal are what contribute to v_C^T. Clearly, if the occupation numbers $\eta_i(t)$ and $\eta_{S,i}$ are very different, then the exact v_C^T, along with its non-adiabatic features, could be relatively large. But if $\eta_i(t)$ and $\eta_{S,i}$ are close enough, then it is possible that the natural orbitals $\psi_i(\mathbf{r},t)$ and KS orbitals could be close enough such that the exact v_C^T is relatively small. Given that the KS occupation numbers are fixed in time, we are then led to test the following question: *If the KS initial state is chosen with occupation numbers close to the true initial state, can the adiabatic approximation qualitatively capture the true dynamics when the time-dependent natural orbitals of the physical system do not evolve significantly in time?* This could cover situations where the system is driven far from any ground-state, since the natural orbitals and KS orbitals could vary significantly in time, while the natural orbital occupation numbers do not change much. We must make an exception for when the dynamics depends critically on the resonant frequencies of the system because generally adiabatic approximations violate the "resonance condition", which is the condition that the resonant frequencies of a system should not change after the system is driven away from its ground-state.[37] Transition amplitudes between states should change but the frequencies themselves should be invariant to the non-equilibrium state the system is left in. This is violated by adiabatic approximations, so that caution must be applied when using TDDFT to examine pump–probe spectra, dynamics that directly depends on resonant frequencies such as for resonantly-driven Rabi oscillations, or dynamics of superposition states evolving freely.

The relation between TD occupation numbers and the exact XC potential was studied earlier in ref. 30, however in a limited sense: the size of the non-adiabatic step features in a range of two-electron model systems, with the KS state taken as a Slater determinant, was shown to correlate with local minima in oscillations of the largest occupation number, regardless of how close the occupation number was to the KS value of 2. In some of these cases, the steps were relatively sharp structures that appeared in regions of low density, so their "force-density", $n(\mathbf{r},t)\nabla v_{XC}(\mathbf{r},t)$, appears less imposing, and further, in some cases they oscillated in time rapidly enough that their influence on the dynamics was relatively small. Non-adiabatic structures beyond global step structures are also important.

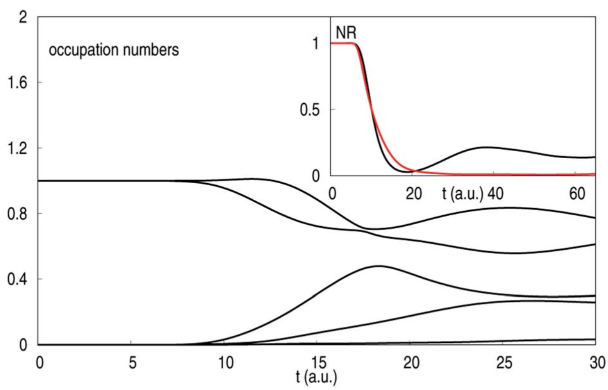

Fig. 2 Time-dependent occupation numbers for the scattering problem. The inset shows the exact (black) and ALDA (red) reflected probability density $N_R(t)$.

Published on 02 June 2020. Downloaded by RUTGERS STATE UNIVERSITY on 9/24/2020 8:27:22 PM.

Published on 02 June 2020. Downloaded by RUTGERS STATE UNIVERSITY on 9/24/2020 8:27:22 PM.

We consider four examples to examine the question above, focusing on propagation with the simplest approximation, ALDA. In seeking examples we have tried to pick a range of different cases (beginning in the ground-state *versus* excited states, field-driven *versus* field-free) where occupation numbers change relatively little for some time but while there is significant dynamics. Our first example returns to the model scattering problem.

2.1 Scattering

The scattering example in Fig. 1 does not depend critically on the satisfaction of the resonant condition, and since the initial KS state chosen $\Phi(0) = \Psi(0)$, the initial KS and true occupation numbers are identical. The fact that the dynamics from the adiabatic approximations does not qualitatively reproduce the true dynamics suggests that the true occupation numbers change significantly over time. This expectation is borne out, as evident in Fig. 2 where one sees large deviations of the occupation numbers at times where the incoming electron density approaches the target. Before this time, the deviation is relatively small, and the dynamics from the adiabatic approximations are qualitatively reasonable (snapshots in ref. 10 and 33); for example, in ALDA, there is an over-spreading of the density, but it does roughly capture the exact dynamics, and ALDA does very well when averaged quantities are considered such as the reflection probability $N_R = \int_{-5}^{\infty} n(x,t)\mathrm{d}x$, as shown in the inset, until the occupation numbers of the physical system begin to significantly change.

We note that in this example, the two occupation numbers beginning with a value of 1 correspond to the incoming electron's orbital and the target electron's orbital. The state is a double Slater determinant, and could be called strongly correlated, if correlation is measured by how far the occupation numbers are from the Slater determinant values of 0 and 2.

2.2 Superposition states

In this example we consider the field-free evolution of a superposition state of a 1D He atom ($v_{\mathrm{ext}}^{\mathrm{1DHe}}(x) = -1/\sqrt{x^2+1}$). We consider a 20 : 80 superposition of its

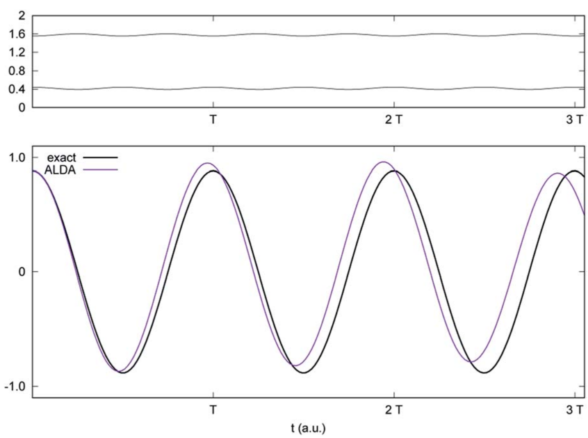

Fig. 3 Time-dependent occupation numbers (upper panel) and exact (black) and ALDA (purple) dipole moments (lower panel) for the superposition state example.

Published on 02 June 2020. Downloaded by RUTGERS STATE UNIVERSITY on 9/24/2020 8:27:22 PM.

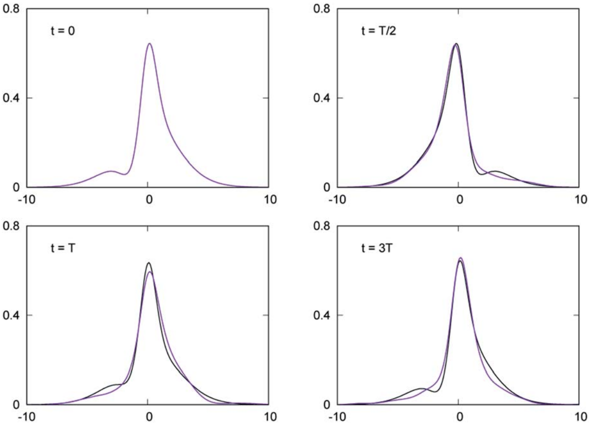

Fig. 4 Snapshots of the exact (black) and ALDA (purple) densities for the superposition state example.

ground and first excited states, $\Psi(0) = (\Psi^{\rm g.s.} + 2\Psi^{\rm e})/\sqrt{5}$, and the freely-evolving density has a periodic dynamics of period $T = 2\pi/(E_{\rm e} - E_{\rm g.s.}) = 11.788$ a.u. There are two dominant initial occupation numbers as shown in Fig. 3, around 1.55 and 0.44, neither of which evolve further than about 0.049 from their initial values, while the density sloshes back and forth in the well. If we begin in a KS excited state of the same configuration, we find that ALDA propagation of its dipole oscillates with a similar period but there is also a very slow beating period, which is only just visible over the duration shown. The ALDA densities in Fig. 4 also follow closely the exact densities, especially if local details are averaged over. This is an example where the system is far from the ground-state, there is significant dynamics while the occupation numbers do not deviate significantly from their initial values, and (locally-averaged) ALDA predicts the dynamics accurately from a KS initial state chosen with a similar configuration to the exact state, consistent with the suggestion from the exact expression.

Generally however, with freely-evolving superposition states, the violation of the resonance condition[37] mentioned earlier adversely affects the dynamics even when the occupation numbers do not deviate far from their initial values. Dynamics in free evolution is purely dependent on the resonant frequencies of the system; the oscillation periods in the dipole are a direct measure of these frequencies. With adiabatic TDDFT, the XC potential leads to these frequencies being generally different when the system is left in different superposition states:[37] essentially, the time-evolving density gives time-dependence to the instantaneous KS potential and its bare KS frequencies, which is not compensated for correctly in the generalized XC kernel defined for non-equilibrium states. On the other hand, the exact frequencies are invariant to which state the system is in. In the particular case above, and some other linear combinations of the ground and first excited states, there is a relatively small violation of the resonance condition, provided the initial KS state is chosen with a similar configuration to the exact state. The ALDA frequency of the lowest excitation as computed by the linear response from the ground-state is 0.480 a.u., while that computed from the period of oscillation in Fig. 3 is 0.553

 This journal is © The Royal Society of Chemistry 2020

a.u. (interestingly, closer to the exact value of 0.533 a.u.). Thus the violation of the resonance condition is evident, since the approximation should give the same value whatever the initial state is, but not very severe, and in this case, because the violation brings the ALDA value closer to the exact value as compared to that computed from the ground-state, the density dynamics is quite well reproduced. We found that when we tried to make more general superposition states, especially with two excited states, ALDA dynamics was very poor due to the violation of the resonance condition, with several frequencies appearing in the ALDA dynamics instead of one, even when the occupation numbers did not change much in time and the initial KS state was chosen to have a similar configuration to, or be identical to, the true initial state.

2.3 Laser-driven ground-state

Here we consider an example where we begin in the ground-state of our 1D He atom and drive it with a non-perturbative non-resonant electric field. The system begins weakly-correlated, in contrast to the previous examples, as indicated by the largest occupation number beginning at 1.98, with the others all below 0.02. Unless otherwise stated, we choose the initial KS state to be identical to the physical state, which gives practically the same dynamics as starting in a Slater determinant with the exact initial density as the true state.

In Fig. 5, a field $\mathscr{E}(t) = 0.5\ \sin(t)$ is linearly turned on over the first 20 a.u. and then held constant. After some time there is a significant change in the occupation numbers and large amplitude dipole oscillations are observed, yet the ALDA dipole plotted in this figure appears to match the exact dipole very closely. That the dipole paints a much rosier picture than the truth is evident from the densities plotted in Fig. 6. ALDA is very good at first, accurately capturing the density oscillations and the details of the lobes evolving outwards. The system evolves very far from a ground-state during the first 30 a.u. or so, and still ALDA

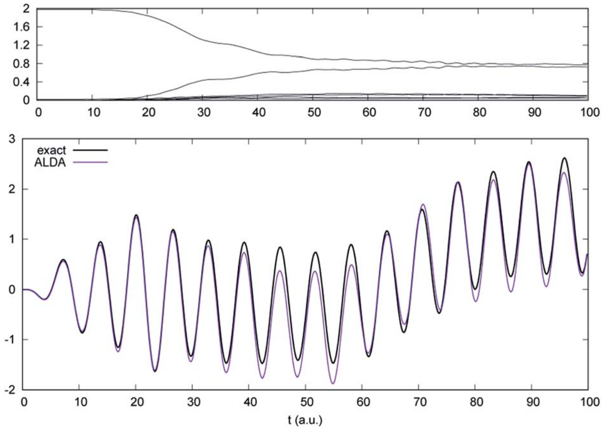

Fig. 5 Time-dependent occupation numbers (top panel) and exact (black) and ALDA (purple) dipole moments (lower panel) for a 1D He ground-state driven with $\mathscr{E}(t) = 0.5\ \sin(t)$ increased over 20 a.u.

Published on 02 June 2020. Downloaded by RUTGERS STATE UNIVERSITY on 9/24/2020 8:27:22 PM.

Published on 02 June 2020. Downloaded by RUTGERS STATE UNIVERSITY on 9/24/2020 8:27:22 PM.

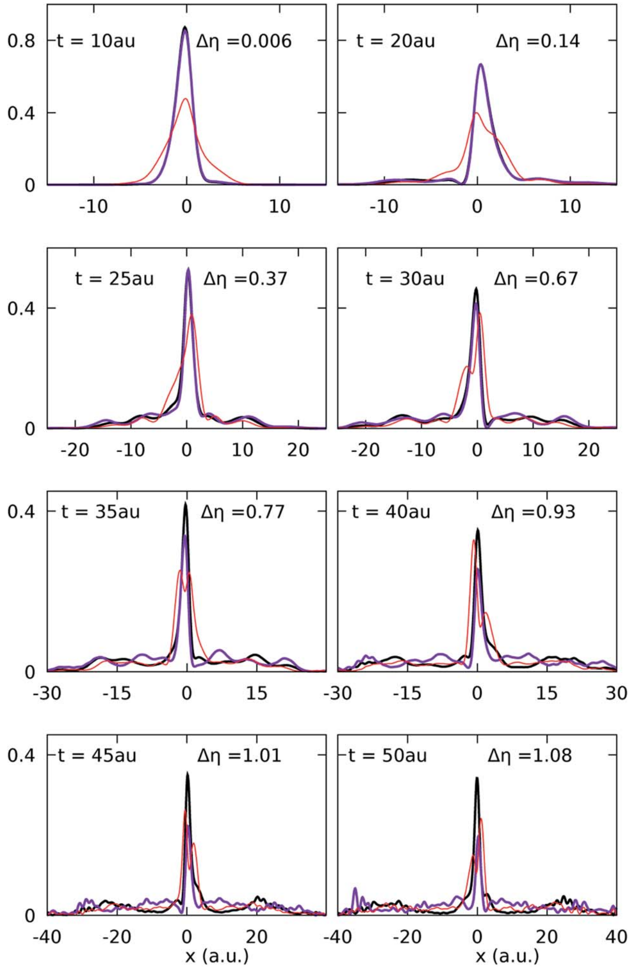

Fig. 6 Snapshots of the exact (black) and ALDA (purple) densities obtained by evolving the 1D He ground-state with $\mathscr{E}(t) = 0.5\ \sin(t)$ increased over 20 a.u. The density evolving from the LDA ground-state propagated using ALDA is shown as the thin red line.

works well provided the initial KS state is a good one, meaning it captures the initial density well. At later times, for example from 35 a.u. onwards, as shown in the figure, the ALDA propagation becomes significantly worse, concomitant with the larger deviation of the dominant occupation number $\Delta\eta$ indicated in the figure. Note that the density becomes increasingly oscillatory in the tails of both the exact and ALDA densities as time evolves due to reflections from the hard-wall boundaries at ±40 a.u. This example also seems to answer our question affirmatively: ALDA predicted a good density dynamics while the deviations of the occupation numbers remained within about 0.5 of their initial values. The importance of having a good initial state is clear, since when the LDA ground-state is propagated instead, the density is considerably worse even at very short times, as evident from the red curves in Fig. 6.

Published on 02 June 2020. Downloaded by RUTGERS STATE UNIVERSITY on 9/24/2020 8:27:22 PM.

2.4 Laser-driven excited state

In our last example, we again begin already far from a ground-state. The same electric field as in the previous example drives the 1D He atom which is now initially in its first excited state. In this case there are two initial natural orbital occupations both within 0.003 of 1, so we start with a KS initial state that is in an excited state configuration of a non-interacting system with the property that the initial density reproduces that of the physical initial state. In fact, taking $\Phi(0) = \Psi(0)$ gave us identical density evolution to starting in the excited KS state. Similar examples in the past[10,35,36] have shown that propagation with an adiabatic approximation on an initial Slater determinant choice for the KS system gives much poorer dynamics than when the KS initial state is chosen with a similar configuration to that of the true system, as also discussed earlier for the scattering example.

The resulting dipole dynamics is accurately captured by ALDA (Fig. 7), however a look at the densities in Fig. 8 shows us that again, globally averaging over the density gives an overly positive picture of the performance of ALDA. The densities show that although the average behavior and density oscillations are well captured in ALDA before the occupation numbers deviate too far, the ALDA density is missing details of the structure, such as the shoulders in the exact densities seen in the top panels of Fig. 8. At the initial time, since the KS initial state is chosen to reproduce the true density, these shoulders are there but ALDA rapidly broadens them and washes them out, even at 5 a.u. Still, if we consider locally averaging over the density of this type of structure, ALDA does quite well even as far as about 25 a.u., after which the largest deviation in the occupation numbers reaches about 0.3, and locally-averaged ALDA develops a more significant error.

In summary, the four examples here illustrate that when the natural occupation numbers remain close to their initial values, ALDA evolution can yield a reasonably accurate density, while errors grow in cases where the occupation numbers deviate significantly from their initial values. It is important to note that the adiabatic approximation performed well even when the system was far from

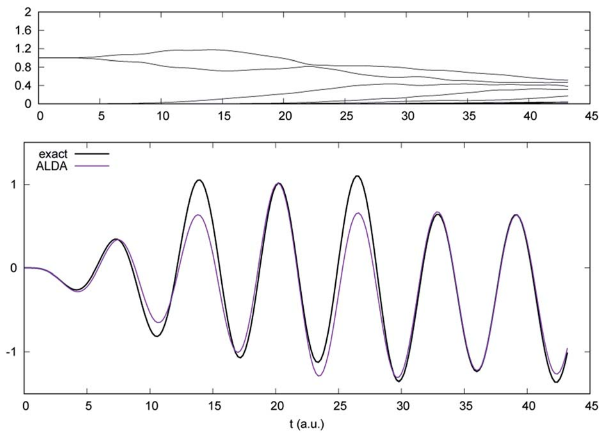

Fig. 7 Time-dependent occupation numbers (upper panel) and exact (black) and ALDA (purple) dipole moments (lower panel) for the laser-driven excited state example.

Published on 02 June 2020. Downloaded by RUTGERS STATE UNIVERSITY on 9/24/2020 8:27:22 PM.

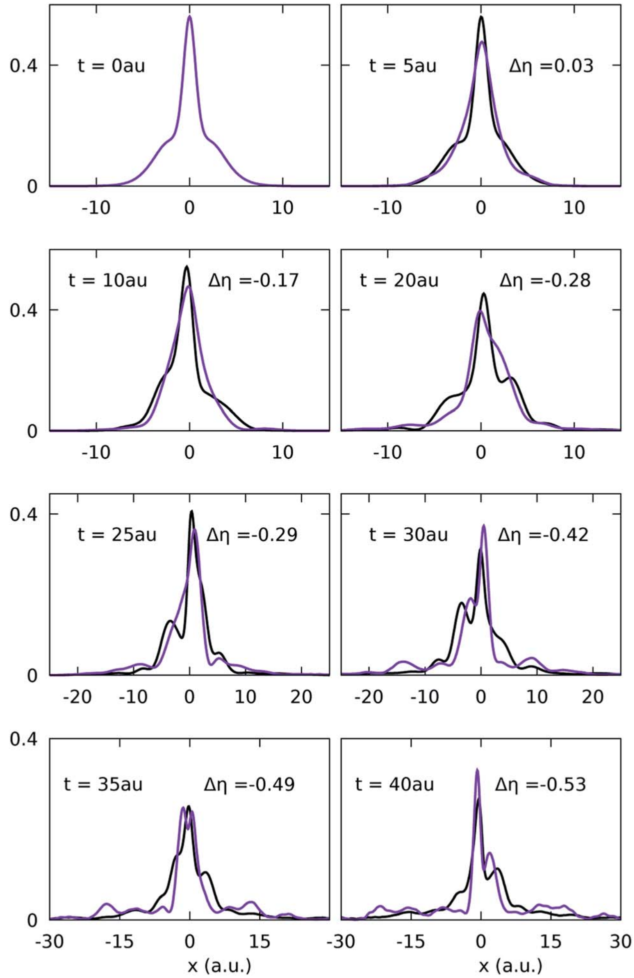

Fig. 8 Snapshots of the exact (black) and ALDA (purple) densities for the laser-driven excited state example. The largest deviation of the occupation number is indicated in each panel as $\Delta\eta$.

any ground-state and key to this is the choice of the KS initial state. We chose the KS initial state to have a configuration very close to that of the true initial state in each case, as earlier work had shown that if this is not the case, adiabatic approximations work much less well; this is clear also from the exact expression for v_{XC}. In some cases globally averaged observables such as the dipole were accurate even when the occupation numbers showed great deviation. Without resorting to a justification in terms of ALDA satisfying a number of exact conditions, this cannot easily be explained from the exact expressions.

3 Density-matrix coupled XC approximations

To go beyond the adiabatic approximation, ref. 32 introduced a class of approximations based on the exact decomposition, eqn (1)–(3). The idea is to use an

Published on 02 June 2020. Downloaded by RUTGERS STATE UNIVERSITY on 9/24/2020 8:27:22 PM.

auxiliary 2RDM $\tilde{\rho}_2$ to approximate the two parts in the expression that are inaccessible from a KS evolution, ρ_1 and n_{XC}. As shown there, the KS equation is considered to be coupled to the first equation of the BBGKY hierarchy that gives an equation for the 1RDM: the 2RDM that appears in this equation is approximated by the auxiliary $\tilde{\rho}_2$ as a functional of the KS wavefunction $\Phi(t)$ and the 1RDM resulting from the BBGKY equation, $\tilde{\rho}_1(t)$. At each time-step, the propagation of the BBGKY equation produces an output $\tilde{\rho}_1$, which, when inserted into eqn (3) and put together with eqn (2) using the XC hole constructed from $\tilde{\rho}_2$, gives a non-adiabatic approximation for v_{XC} that satisfies exact conditions such as the zero-force theorem and the harmonic potential theorem, and captures non-adiabatic step features in the XC potential. The first BBGKY equation and the KS equation should be solved self-consistently, exchanging inputs at each time-step, and it can be shown that such a scheme ensures that propagation yields the same density in each.

For example, one can choose $\tilde{\rho}_2 = \rho_{2,\mathrm{S}}$, an approximation we denoted in ref. 32 as $v_{\mathrm{XC}}^{\tilde{\rho}}$, which results in the interaction component $v_{\mathrm{XC}}^{\mathrm{W}}$ coinciding with $v_{\mathrm{XC}}^{\mathrm{S}}$ and a non-zero kinetic component. Unfortunately, although this first DMXC approximation captured the elusive non-adiabatic structures in model systems, after too short a time the dynamics developed sharp structures that rapidly self-amplified and killed the calculation. It was observed in that work that if a Hartree–Fock (HF) driven calculation was performed instead, where $\tilde{\rho}_2$ is taken to be the HF functional of $\tilde{\rho}_1$, step and peak structures generally appeared in the correlation potential, and the dynamics remained stable. However, as such a calculation simply reproduces the HF density, it is not of practical use (in the special case of two electrons in a KS state which is a doubly-occupied spatial orbital, HF propagation would reduce to exact exchange, which is adiabatic and has no step structures if the initial $\tilde{\rho}_1(0)$ is chosen to coincide with the KS 1RDM. Choosing it to be the true $\rho_1(0)$ of the interacting system, however, does generate a step structure).

Still, the observation raises the possibility of using a "hybrid" $\tilde{\rho}_2$, which is a linear combination of $\rho_{2,\mathrm{S}}$ and $\rho_2^{\mathrm{HF}}[\tilde{\rho}_1]$, with the hope that the HF component tames the instability. Here we test this for the scattering problem discussed in Sec. 1 and 2. We now denote the approximation where $\tilde{\rho}_2 = \rho_{2,\mathrm{S}}$ as $v_{\mathrm{XC}}^{\rho_{2,\mathrm{S}}}$, while we define the hybrid approximation through

$$v_{\mathrm{XC}}^{a\rho_{2,\mathrm{S}}}: \quad \tilde{\rho}_2 = (1-a)\rho_2^{\mathrm{HF}}[\tilde{\rho}_1] + a\rho_{2,\mathrm{S}} \tag{7}$$

with $0 \leq a \leq 1$. For the scattering problem, ref. 32 had shown that $v_{\mathrm{XC}}^{\rho_{2,\mathrm{S}}}$ captures a peak/step-like increase behind the target that develops when the incoming electron begins to meet the target, which plays an important role in delaying the transit of the incoming electron through the target, allowing more correlation with the target. The ALDA, $v_{\mathrm{XC}}^{\mathrm{S}}$, and other adiabatic approximations studied in ref. 10 did not have this structure, with resulting densities with larger tails on the other side of the target. But $v_{\mathrm{XC}}^{\rho_{2,\mathrm{S}}}$ continues for only a short time beyond this, failing after about 12 a.u, before there is appreciable reflection.

In Fig. 9 we see that the numerical stability is improved as the amount of $\rho_2^{\mathrm{HF}}[\tilde{\rho}_1]$ included in the approximation increases; $v_{\mathrm{XC}}^{0.8\rho_{2,\mathrm{S}}}$ which included 0.2 HF propagated for 12.2 a.u. before the instability killed it, $v_{\mathrm{XC}}^{0.5\rho_{2,\mathrm{S}}}$ propagated for 13.8 a.u., and $v_{\mathrm{XC}}^{0.2\rho_{2,\mathrm{S}}}$ propagated until the end of the simulation. At early times (first panel in the figure), before there is much overlap between the incoming electron

Published on 02 June 2020. Downloaded by RUTGERS STATE UNIVERSITY on 9/24/2020 8:27:22 PM.

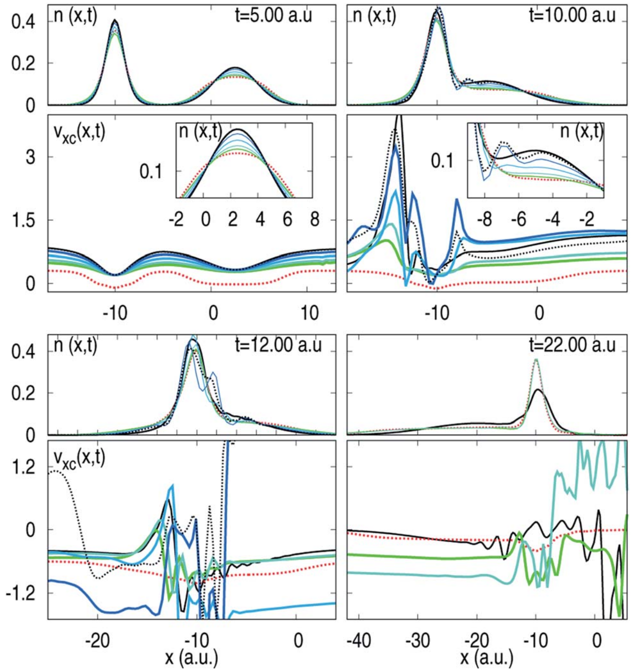

Fig. 9 Snapshots of the exact (black solid line) and ALDA (red dotted line) density and XC potential, and those computed with the density-matrix coupled approximations with different ratios of $\rho_{2,S}$ and $\rho_2[\tilde{\rho}_1]$: $v_{XC}^{0\rho_{2,S}}$ (light green), $v_{XC}^{0.2\rho_{2,S}}$ (dark green), $v_{XC}^{0.5\rho_{2,S}}$ (light blue), $v_{XC}^{0.8\rho_{2,S}}$ (dark blue) and $v_{XC}^{\rho_{2,S}}$ (black dotted). Insets at time $t = 5.00$ a.u. and $t = 10.00$ a.u. show zoomed images of the density in the regions with the largest differences.

and the target, the approximations with larger a, *i.e.* larger fraction of $\rho_{2,S}$ and less $\rho_2^{HF}[\tilde{\rho}_1]$, are the best, with the XC potentials also being a better approximation of the exact potentials for larger a. Actually, at these early times, ref. 10 and 33 showed that v_{XC}^{S}, which completely neglects v_C^T and approximates v_{XC}^W by using the KS hole in place of the true hole, also does almost perfectly, in contrast to ALDA (and adiabatic exact exchange) which give densities that are too spread out. As the incoming electron's density begins to overlap more with the target (second panel), the densities in the target region and also just behind it are better approximated the larger the fraction of $\rho_{2,S}$ included. At these times a crucial role is played by the peak structure that develops early behind the target, as mentioned above. When HF dilutes the approximation, this peak is subdued, as evident in the plot of the potentials, and the effect of the increased interaction time is diminished. However, the approximations that manage to survive for times long enough to witness reflection do not contain enough $\rho_{2,S}$: their predominantly HF nature is unable to capture the important persistent step structure down to the right of the center of the target ($x = -10$ a.u.) that develops soon after 20 a.u. and is crucial for reflecting the electron back to the right and as a result, the reflection result is not improved. Even though these approximations contain a lot of structure, they rapidly vary in space and time such that there is no significant impact on the resulting dynamics (in contrast to the persistent step down structure in the exact potential, see ESI Movie of ref. 10).

This journal is © The Royal Society of Chemistry 2020

Published on 02 June 2020. Downloaded by RUTGERS STATE UNIVERSITY on 9/24/2020 8:27:22 PM.

Thus, although the "hybrid" non-adiabatic approximation is able to stabilize the calculation for longer times, and non-adiabatic structures are captured if the fraction of HF is not too large, the fraction of HF needed to stabilize the calculation for long enough times to witness reflection is too large compared to the $\rho_{2,\mathrm{S}}$ component such that non-adiabatic features get lost. Indeed, as we see in Fig. 9 at time $t = 22$ a.u., the density remaining at the target is almost the same for $v_{\mathrm{XC}}^{0.2\rho_{2,\mathrm{S}}}$, ALDA, and HF, whereas the exact calculation shows a smaller and more spread out density, resulting from reflection and an energy transfer between the target and the incoming wavepacket.

4 Coupling-constant integrations

Finding an adequate approximation for $v_{\mathrm{C}}^{\mathrm{T}}$ is challenging, as evident from the above sections. Here we consider whether there is a way to "hide" this kinetic contribution to correlation in a coupling-constant integral, analogous to the adiabatic connection expression for the XC energy[38,39] in ground-state DFT.

The notion of coupling-constant connection was introduced in TDDFT in ref. 40 where it was used to develop a perturbation theory for v_{XC}. Here instead we search for a coupling-constant integral expression which usurps $v_{\mathrm{C}}^{\mathrm{T}}$. We consider then the Hamiltonian

$$H^{\lambda} = T + \lambda W + V^{\lambda}(t) \tag{8}$$

where the coupling-constant λ is a parameter taking us from the KS system at $\lambda = 0$ to the true system at $\lambda = 1$, while the density $n^{\lambda}(\mathbf{r},t) = n(\mathbf{r},t)$ for all values of λ. We have

$$H^{\lambda}\Psi^{\lambda}(t) = i\partial_t\Psi^{\lambda}(t),\; n_{\Psi^{\lambda}}(\mathbf{r},t) = n(\mathbf{r},t) \tag{9}$$

with the initial state for each λ, $\Psi^{\lambda}(0)$, being freely chosen with the only restriction that its initial density and the initial first-time derivative of its density are equal to those of the true wavefunction, $\Psi^{\lambda=1}(0) = \Psi(0)$. Unlike in the ground-state case, due to the initial state freedom, there are an infinite number of possible coupling-constant paths for a given choice of KS initial state, $\Psi^{\lambda=0}(0) = \Phi(0)$, as illustrated in the cartoon in Fig. 10. The hope is then to express

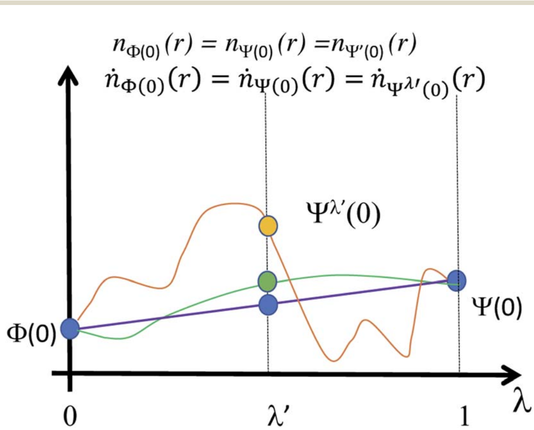

Fig. 10 Sketch of three different possible coupling-constant paths for the time-dependent case (see text).

$$v_{XC}[n;\Psi(0),\Phi(0)](\mathbf{r},t)=\int_0^1 f(\lambda)\mathrm{d}\lambda \tag{10}$$

where the kinetic term no longer appears, but instead is usurped by the coupling-constant integral. Different components of $f(\lambda)$ will look completely different for different coupling-constant paths, yet the total integral will be the same. Here we do not discuss the question of the existence of a given path in λ, and simply assume that the initial λ-path can be propagated, remaining v-representable and differentiable with respect to λ at every time. We note that this freedom of the path in λ is distinct from the freedom of choice of the initial KS state, that is, for a given physical initial state $\Psi(0)$, there are infinitely many possible initial KS states $\Phi(0)$, each of which gives a different $v_{XC}(\mathbf{r},t)$.

In the ground-state case, the adiabatic connection expression for the XC energy eliminates the kinetic contribution by taking the λ-derivative of the expectation value of the energy, making use of the Hellmann–Feynman theorem, and then integrating over $\lambda = 0$ to 1. Here in the time-dependent case, we consider instead the integral that follows from evaluating the Lagrangian action at λ on the solution to eqn (9):

$$A^\lambda=\int_0^T \mathrm{d}t'\left\langle\Psi^\lambda(t')\middle|i\partial_{t'}-\hat{H}^\lambda\middle|\Psi^\lambda(t')\right\rangle=0. \tag{11}$$

Computing the integrand of the left-hand-side of

$$\int_0^1 \mathrm{d}\lambda\frac{\partial}{\partial\lambda}A^\lambda=A^{\lambda=1}-A^{\lambda=0}=0, \tag{12}$$

eliminates the kinetic term in the Hamiltonian, and after some manipulations, we arrive at

$$\begin{aligned}\int_0^T \mathrm{d}t'\int \mathrm{d}r' v_{XC}(r',t')n(r',t')=\frac{1}{2}\int_0^T \mathrm{d}t'\iint \mathrm{d}r_1\mathrm{d}r_2 w(r_1,r_2)\overline{n_{XC}^\lambda(r_1,r_2;t')}n(r_1,t')\\ -\int_0^T U[n(t')]\mathrm{d}t'+\left(\overline{\left\langle\Psi^\lambda(T)\middle|-i\frac{\partial}{\partial\lambda}\Psi^\lambda(T)\right\rangle}-\overline{\left\langle\Psi^\lambda(0)\middle|-i\frac{\partial}{\partial\lambda}\Psi^\lambda(0)\right\rangle}\right)\end{aligned} \tag{13}$$

where $U[n]$ is the Hartree energy and the overline notation denotes the coupling-constant integral $\bar{f}=\int_0^1 f(\lambda)\mathrm{d}\lambda$. Applying now the functional derivative, $\frac{\delta}{\delta n(\mathbf{r},t)}$ where $0 < t < T$, to eqn (13) yields

$$\begin{aligned}v_{XC}(r,t)=&-\int_0^T \mathrm{d}t'\int \mathrm{d}r' f_{XC}\left(r',t';r,t\right)n\left(r',t'\right)-v_H(r,t)\\ &+\frac{\delta}{\delta n(r,t)}\left(\overline{\left\langle\Psi^\lambda(T)\middle|-i\frac{\partial}{\partial\lambda}\Psi^\lambda(T)\right\rangle}-\overline{\left\langle\Psi^\lambda(0)\middle|-i\frac{\partial}{\partial\lambda}\Psi^\lambda(0)\right\rangle}\right)\\ &+\frac{1}{2}\int_0^T \mathrm{d}t'\iint \mathrm{d}r_1\mathrm{d}r_2 w(r_1,r_2)\left[\frac{\delta}{\delta n(r,t)}\overline{n_{XC}^\lambda\left(r_1,r_2;t'\right)}\right]n\left(r_1,t'\right)\\ &+\frac{1}{2}\int \mathrm{d}r_2 w(r,r_2)\overline{n_{XC}^\lambda(r,r_2;t)}\end{aligned} \tag{14}$$

Published on 02 June 2020. Downloaded by RUTGERS STATE UNIVERSITY on 9/24/2020 8:27:22 PM.

Published on 02 June 2020. Downloaded by RUTGERS STATE UNIVERSITY on 9/24/2020 8:27:22 PM.

where $f_{\mathrm{XC}}(r',t';r,t) = \dfrac{\delta v_{\mathrm{XC}}(r',t')}{\delta n(r,t)}$ is a generalized linear response kernel, measuring the response of the XC potential at time t' to a density perturbation at time t. Given that $0 < t < T$ and that v_{XC} is a causal function, there is a significant amount of cancellation between the terms. Making use of causality and taking $T = t^{+}$, we write

$$\begin{aligned} v_{\mathrm{XC}}(r,t) = &-\int_t^{t^+} \mathrm{d}t' \int \mathrm{d}r' f_{\mathrm{XC}}(r',t';r,t) n(r',t') - v_{\mathrm{H}}(r,t) \\ &+ \frac{1}{2}\int \mathrm{d}r_2 w(r,r_2)\overline{n_{\mathrm{XC}}^{\lambda}(r,r_2;t)} + \frac{\delta}{\delta n(r,t)}\overline{\left\langle \Psi^{\lambda}(t) \middle| -i\frac{\partial}{\partial\lambda}\Psi^{\lambda}(t)\right\rangle} \\ &+ \frac{1}{2}\int_t^{t^+} \mathrm{d}t' \iint \mathrm{d}r_1 \mathrm{d}r_2 w(r_1,r_2)\left[\frac{\delta}{\delta n(r,t)}\overline{n_{\mathrm{XC}}^{\lambda}(r_1,r_2;t')}\right] n(r_1,t'). \end{aligned} \tag{15}$$

It may appear that by trying to avoid computing and approximating the challenging term $v_{\mathrm{C}}^{\mathrm{T}}$, we have jumped from the frying pan into the fire. Perhaps the hottest flames come from the term involving the density-functional derivative of the coupling-constant integral of the wavefunction projection of the λ-derivative of the wavefunction.

In fact, considering the ground-state limit of this expression sheds some light on this term. Returning momentarily to eqn (13), and taking $\Psi^{\lambda}(t) = \mathrm{e}^{-iE_0^{\lambda}t}\Psi_0^{\lambda}$ with the eigenstate satisfying $(T + V^{\lambda} + \lambda W)\Psi_0^{\lambda} = E_0^{\lambda}\Psi_0^{\lambda}$, it is straightforward to compute

$$\begin{aligned} &\frac{1}{T}\left(\overline{\left\langle \Psi^{\lambda}(T) \middle| -i\frac{\partial}{\partial\lambda}\Psi^{\lambda}(T)\right\rangle} - \overline{\left\langle \Psi^{\lambda}(0) \middle| -i\frac{\partial}{\partial\lambda}\Psi^{\lambda}(0)\right\rangle}\right) \\ &= E_0^{\lambda=0} - E_0^{\lambda=1} = \int \mathrm{d}r' v_{\mathrm{XC}}(r',t') n(r',t') + U[n] - E_{\mathrm{XC}}[n] \end{aligned}$$

which resolves the rather unusual appearance of the Hartree energy in eqn (13), and the Hartree potential in eqn (15). Using the fact that $E_0^{\lambda=1} = T_{\mathrm{s}}[n] + U[n] + E_{\mathrm{XC}}[n] + \int \mathrm{d}r' v_{\mathrm{ext}}(r',t') n(r',t')$ is the true physical energy, and that $E_0^{\lambda=0} = T_{\mathrm{s}}[n] + \int \mathrm{d}r' v_{\mathrm{ext}}(r',t') n(r',t') + \int \mathrm{d}r' v_{\mathrm{H}}(r',t') n(r',t') + \int \mathrm{d}r' v_{\mathrm{XC}}(r',t') n(r',t')$ is the sum of the KS eigenvalues, this retrieves the ground-state adiabatic connection formula, $E_{\mathrm{XC}}[n] = \dfrac{1}{2}\iint \mathrm{d}r_1 \mathrm{d}r_2 w(r_1,r_2)\overline{n_{\mathrm{XC}}^{\lambda}(r_1,r_2)} n(r_1)$.

It can also be shown that in the general time-dependent case, there is some cancellation between the Berry-like term and the other terms in eqn (15) including the Hartree potential. The question then is how to approximate this term and the others in order to get a good practical approximation for v_{XC}. What would be most desirable is to somehow extract out adiabatic terms, and approximate the rest. This term should not be considered in isolation from the last two terms in eqn (15), since different coupling-constant integration paths (see Fig. 10) weight the terms differently, yet their sum is the same.

This is but one possible coupling-constant formula. There are other paths one could follow, for example considering the action for a fixed potential as a functional of the density,[41] or making a coupling-constant path between the adiabatic approximation and the exact expression, which would give a formula

Published on 02 June 2020. Downloaded by RUTGERS STATE UNIVERSITY on 9/24/2020 8:27:22 PM.

directly for the memory-dependent part of v_{XC} as a correction to the adiabatic approximation through coupling-constant integration. Future work will also consider whether the scaling relations derived in ref. 42 could be used to approximately evaluate some of these terms.

5 Conclusions and outlook

This paper has explored three different lines of functional development in TDDFT: whether one can characterize the accuracy of adiabatic TDDFT by considering how strongly the natural orbital occupation numbers evolve in time, how one can use a decomposition of the exact XC potential to develop density-matrix coupled XC approximations, and an introduction of the idea of memory-dependent functionals based on coupling-constant integration.

The first part paints a partially reassuring picture of the use of adiabatic approximation, in that the range of validity of ALDA appears wider than the weak perturbations of the ground-state. On the other hand this seems to be limited to the cases where occupation numbers do not change significantly during the dynamics which can be hard to predict in practice. It should also be noted that in some applications the external field dominates over XC effects in driving the dynamics, and it could well be that in many applications on realistic systems where the occupation numbers vary significantly and yet the adiabatic approximation works well, the essential role of XC is to partially counter self-interaction in the Hartree potential, sometimes even just at the ground-state level.

From our density-matrix coupled approximation we learned that the structure of the force balance equations for the exact potential, especially for v_C^T, seems to naturally generate the non-adiabatic features even when the exact 1RDM is replaced by a relatively simple approximation. This gives us hope for the possible development of approximations based on this expression. Also, even if the particular choices for the 1RDM explored here lead to a numerically unstable approach, the derivation of a linear-response exchange–correlation kernel is still possible, and could provide useful insights. Moreover, linear-response calculations should limit the possibility of numerical instabilities.

Of course, the perfect solution to the difficulty of modeling v_C^T would be to get rid of this term altogether, using a coupling-constant integration, as in the final part of this paper. While it is not clear what nor how approximations could be obtained from the expression presented here, it opens up a new avenue for future derivations of non-adiabatic functionals for TDDFT.

Conflicts of interest

There are no conflicts to declare.

Acknowledgements

Financial support from the US National Science Foundation CHE-1940333 (N. T. M.) and the Department of Energy, Office of Basic Energy Sciences, Division of

Chemical Sciences, Geosciences and Biosciences under Award DE-SC0020044 (L. L.) is gratefully acknowledged.

Published on 02 June 2020. Downloaded by RUTGERS STATE UNIVERSITY on 9/24/2020 8:27:22 PM.

Notes and references

1 E. Runge and E. K. U. Gross, *Phys. Rev. Lett.*, 1984, **52**, 997–1000.
2 N. T. Maitra, *J. Chem. Phys.*, 2016, **144**, 220901.
3 *Fundamentals of time-dependent density functional theory*, ed. M. A. Marques, N. T. Maitra, F. M. Nogueira, E. K. Gross and A. Rubio, Springer, 2012, vol. 837.
4 C. A. Ullrich, *Time-dependent density-functional theory: concepts and applications*, Oxford University Press, 2011.
5 L. D. M. Peters, J. Kussmann and C. Ochsenfeld, *J. Chem. Theory Comput.*, 2019, **15**, 6647–6659.
6 E. W. Draeger, X. Andrade, J. A. Gunnels, A. Bhatele, A. Schleife and A. A. Correa, *J. Parallel Distr. Com.*, 2017, **106**, 205–214.
7 P. Elliott, J. I. Fuks, A. Rubio and N. T. Maitra, *Phys. Rev. Lett.*, 2012, **109**, 266404.
8 J. Ramsden and R. Godby, *Phys. Rev. Lett.*, 2012, **109**, 036402.
9 J. I. Fuks, P. Elliott, A. Rubio and N. T. Maitra, *J. Phys. Chem. Lett.*, 2013, **4**, 735–739.
10 Y. Suzuki, L. Lacombe, K. Watanabe and N. T. Maitra, *Phys. Rev. Lett.*, 2017, **119**, 263401.
11 F. Covito, E. Perfetto, A. Rubio and G. Stefanucci, *Phys. Rev. A*, 2018, **97**, 061401.
12 N. Dittmann, J. Splettstoesser and N. Helbig, *Phys. Rev. Lett.*, 2018, **120**, 157701.
13 C. Verdozzi, *Phys. Rev. Lett.*, 2008, **101**, 166401.
14 V. Kapoor, *Phys. Rev. A*, 2016, **93**, 063408.
15 S. Raghunathan and M. Nest, *J. Chem. Theory Comput.*, 2011, **7**, 2492–2497.
16 R. Ramakrishnan and M. Nest, *Phys. Rev. A*, 2012, **85**, 054501.
17 S. Raghunathan and M. Nest, *J. Chem. Theory Comput.*, 2012, **8**, 806–809.
18 B. F. Habenicht, N. P. Tani, M. R. Provorse and C. M. Isborn, *J. Chem. Phys.*, 2014, **141**, 184112.
19 H. O. Wijewardane and C. A. Ullrich, *Phys. Rev. Lett.*, 2008, **100**, 056404.
20 C.-Z. Gao, P. M. Dinh, P.-G. Reinhard and E. Suraud, *Phys. Chem. Chem. Phys.*, 2017, **19**, 19784–19793.
21 C. A. Ullrich, *J. Chem. Phys.*, 2006, **125**, 234108.
22 C. A. Rozzi, *Nat. Commun.*, 2013, **4**, 1602.
23 A. Bruner, S. Hernandez, F. Mauger, P. M. Abanador, D. J. LaMaster, M. B. Gaarde, K. J. Schafer and K. Lopata, *J. Phys. Chem. Lett.*, 2017, **8**, 3991–3996.
24 P. Elliott, T. Müller, J. K. Dewhurst, S. Sharma and E. Gross, *Sci. Rep.*, 2016, **6**, 38911.
25 S. Yamada, M. Noda, K. Nobusada and K. Yabana, *Phys. Rev. B*, 2018, **98**, 245147.
26 T. T. Gorman, T. D. Scarborough, P. M. Abanador, F. Mauger, D. Kiesewetter, P. Sándor, S. Khatri, K. Lopata, K. J. Schafer, P. Agostini, M. B. Gaarde and L. F. DiMauro, *J. Chem. Phys.*, 2019, **150**, 184308.

Published on 02 June 2020. Downloaded by RUTGERS STATE UNIVERSITY on 9/24/2020 8:27:22 PM.
27 J. I. Fuks, L. Lacombe, S. E. B. Nielsen and N. T. Maitra, *Phys. Chem. Chem. Phys.*, 2018, **20**, 26145–26160.
28 L. O. Wagner, Z.-h. Yang and K. Burke, in *Exact Conditions and Their Relevance in TDDFT*, ed. M. A. Marques, N. T. Maitra, F. M. Nogueira, E. Gross and A. Rubio, Springer Berlin Heidelberg, Berlin, Heidelberg, 2012, pp. 101–123.
29 R. van Leeuwen, *Phys. Rev. Lett.*, 1999, **82**, 3863.
30 K. Luo, J. I. Fuks, E. D. Sandoval, P. Elliott and N. T. Maitra, *J. Chem. Phys.*, 2014, **140**, 18A515.
31 M.-L. M. Tchenkoue, M. Penz, I. Theophilou, M. Ruggenthaler and A. Rubio, *J. Chem. Phys.*, 2019, **151**, 154107.
32 L. Lacombe and N. T. Maitra, *J. Chem. Theory Comput.*, 2019, **15**, 1672–1678.
33 L. Lacombe, Y. Suzuki, K. Watanabe and N. T. Maitra, *Eur. Phys. J. B*, 2018, **91**, 96.
34 Y. Lee, X. Yao, M. V. Fischetti and K. Cho, *Phys. Chem. Chem. Phys.*, 2020, **22**, 8616.
35 J. I. Fuks, S. Nielsen, M. Ruggenthaler and N. T. Maitra, *Phys. Chem. Chem. Phys.*, 2016, **18**, 20976.
36 P. Elliott, J. I. Fuks, A. Rubio and N. T. Maitra, *Phys. Rev. Lett.*, 2012, **109**, 266404.
37 J. I. Fuks, K. Luo, E. D. Sandoval and N. T. Maitra, *Phys. Rev. Lett.*, 2015, **114**, 183002.
38 O. Gunnarsson and B. I. Lundqvist, *Phys. Rev. B: Solid State*, 1976, **13**, 4274–4298.
39 J. P. Perdew and S. Kurth, in *Density Functionals for Non-relativistic Coulomb Systems in the New Century*, ed. C. Fiolhais, F. Nogueira and M. A. L. Marques, Springer Berlin Heidelberg, Berlin, Heidelberg, 2003, pp. 1–55.
40 A. Görling, *Phys. Rev. A: At., Mol., Opt. Phys.*, 1997, **55**, 2630–2639.
41 G. Vignale, *Phys. Rev. A: At., Mol., Opt. Phys.*, 2008, **77**, 062511.
42 P. Hessler, J. Park and K. Burke, *Phys. Rev. Lett.*, 1999, **82**, 378–381.

This journal is © The Royal Society of Chemistry 2020